Quantifying Tortuosity of Porous Li-Ion Battery Electrodes: Comparing Polarization-Interrupt and Blocking-Electrolyte Methods

Fezzeh Pouraghajan,[1,*] Hannah Knight,[1] Michael Wray,[1] Brian Mazzeo,[2] Ram Subbaraman,[3] Jake Christensen,[3] and Dean Wheeler[1,,z]**

[1]*Department of Chemical Engineering, Brigham Young University, Provo, Utah 84602, USA*
[2]*Department of Electrical & Computer Engineering, Brigham Young University, Provo, Utah 84602, USA*
[3]*Robert Bosch LLC, Research and Technology Center, Palo Alto, California 94304, USA*

Ionic mass transport including electrolyte diffusivity and conductivity depends on the geometric tortuosity of the electrode. This paper compares two experimental methods that determine tortuosity based on diffusivity or conductivity. The polarization-interrupt method previously developed by our group determines tortuosity in terms of effective diffusivity. The blocking-electrolyte method proposed by Gasteiger and coworkers determines tortuosity in terms of effective ionic conductivity and is analyzed using a generalized transmission-line model to account for multiple sources of impedance. Tortuosity of several commercial-quality electrodes was measured using both methods, producing reasonable agreement between the two methods in most cases. The advantages and disadvantages of each method and variables that can affect the accuracy of the measurement, such as electrode wetting and model fitting, are discussed. For particular electrodes, one method may be advantageous or more conveniently applied than the other.
 [DOI: 10.1149/2.0611811jes]

Manuscript submitted April 27, 2018; revised manuscript received August 2, 2018. Published August 22, 2018. This was Paper 135 presented at the New Orleans, Louisiana, Meeting of the Society, May 28-June 1, 2017.

Since their invention, Li-ion batteries have been the subject of much research because of their high energy density and promise for further improvement. In spite of substantial progress in this field, designing safe and high-capacity batteries with low cost and high longevity is still challenging. Developing new battery materials and optimizing electrode microstructure are effective ways that batteries can achieve higher capacities and high-rate performance.[1–5] One way to improve the battery's performance, relevant to this work, is to enhance electronic and ionic transport within the electrodes. An important step to optimize electronic and ionic transport properties within the battery's porous electrodes is to accurately understand each of these quantities and their relationships to the complex microstructure of the electrode. The effects of microstructure on performance are particularly evident when operating a cell at high current in which mass transport is more likely to limit performance.

Tortuosity and porosity are two simple parameters that can be used to summarize the complex microstructure of electrodes. The concept of tortuosity (τ) has differing definitions in literature. One definition of tortuosity is the ratio between the shortest pathway for mass transfer between two points and the straight distance between those points. This definition disregards the effect of non-uniform cross-sectional area of the pathway (Figure 1, pathway c). Another common definition for tortuosity—used in this work—is described by the following equations:

$$D_{\text{eff}} = \frac{\epsilon}{\tau} D \qquad [1]$$

$$k_{\text{eff}} = \frac{\epsilon}{\tau} k_{\text{int}} \qquad [2]$$

where ϵ is the porosity, D_{eff} and D are the effective and intrinsic diffusivity, respectively, and k_{eff} and k_{int} are effective and intrinsic conductivity, respectively. "Intrinsic" means the property of the pure electrolyte (filling 100% of the volume) and "effective" means the measured property of the electrolyte when it is filled within a porous structure. The ratio τ/ϵ is also known as the MacMullin number (N_{M}).

Tortuosity is an important input parameter in mathematical models of battery performance. These mathematical models are useful tools that provide an understanding of the kinetics and transport properties of batteries, hence predicting the performance or failure of battery cells in a way that is less expensive than, or not accessible through, actual experiments. The most famous class of models originate with John Newman and coworkers.[6] These models account for the behavior of solid and liquid phases through solving differential equations in 1D. Such models can be used to explain the effect of microstructure on the macroscopic behavior. The accuracy of these models depends in part upon the accuracy of the tortuosity input parameter used.

In order to estimate tortuosity for use in computer models of battery performance, the Bruggeman relationship is most commonly used.[7]

$$\tau = \epsilon^{\alpha} \qquad [3]$$

where α is the Bruggeman exponent, commonly taken to be -0.5.[8,9] Experimental evidence, however, shows that the Bruggeman relationship can significantly under predict tortuosity for porous battery electrodes.[10]

For measuring or calculating tortuosity, there are various methods in the field of electrochemistry.[11] These include: AC impedance-based techniques,[12–15] a method based on gas diffusion measurement,[16] and 3D visualization techniques, including X-ray tomography and focused-ion beam scanning electron microscope tomography (FIB/SEM), coupled with computational models.[17–22] One drawback to the gas diffusion measurement is that the measurement of in-plane

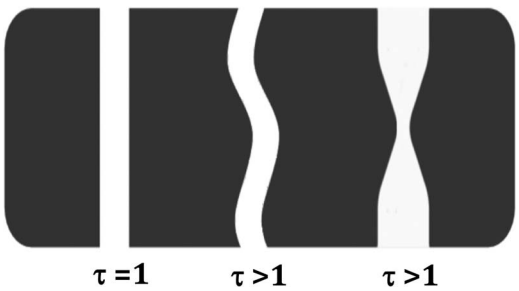

Figure 1. Representation of tortuous pathways.

*Electrochemical Society Student Member.
**Electrochemical Society Member.
zE-mail: dean_wheeler@byu.edu

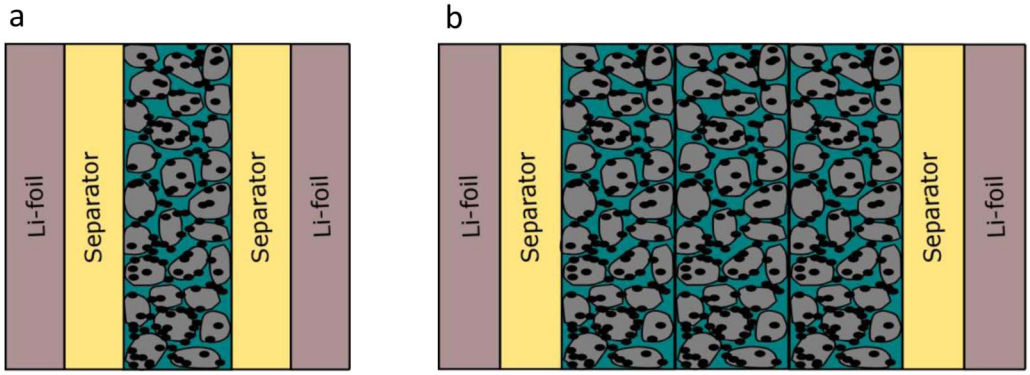

Figure 2. a) Schematic of (a) a typical polarization-interrupt cell (b) cell used for measuring relatively low tortuosity films.

diffusivity may not match through-plane diffusivity if the electrodes are not isotropic—in contrast, the present work is focused on through-plane transport measurements, which are more relevant to battery performance. 3D visualization techniques are limited by the difficulty of detecting carbon and binder using X-ray tomography since carbon and binder have a significant effect on ion transport.[23] These techniques are further limited by the relatively small volume that SEM/FIB images can access. These drawbacks were partially addressed by Thiele and coworkers[19] who combined the methods of SEM/FIB to determine carbon and binder distribution and X-ray tomography to obtain active material distribution, taking advantage of both methods of 3D visualization. While this is effective, it requires a considerable amount of effort and is nevertheless not a direct measurement of tortuosity.

In this work we compare two methods for direct measurement of the tortuosity of thin-film electrodes: the polarization-interrupt method (DC method) previously developed by our group,[10,24] and the blocking-electrolyte method (AC impedance method) developed by Gasteiger and coworkers,[12] Building on this prior work, a generalized transmission line model, comparable to that developed by Troltzch and Kanoun,[25] and Göhr[26] is presented here and used as part of the blocking-electrolyte method in order to take into account multiple sources of impedance. The overall objective is to find the limits of applicability of the two methods and how well they agree for the tortuosity of realistic Li-ion battery electrodes.

Polarization-Interrupt Method

The polarization-interrupt experiment is combined with a transport model and used to measure effective electrolyte transport in porous films.[10,24] Equation 1 is used to determine either tortuosity or MacMullin number from a measurement of the ratio of effective diffusivity to intrinsic diffusivity.

The type of cell used for this experiment is a symmetric cell made by taking a freestanding electrode film, prepared by delaminating the electrode (separating from current collector), and sandwiching it first between two separators and then between two lithium foils pressed onto copper current collectors, which serve as the electrodes for the symmetric cell. Figure 2a shows the schematic of the cell.

The experiment begins by passing a fixed direct current across the cell. After a 2-minute polarization period, the current is then 'interrupted', by turning it off. During the polarization, a concentration gradient is created in the cell by generating Li^+ ions at one electrode and consuming Li^+ ions at the other. A concentration gradient across the cell results in a measureable concentration over-potential. After interruption of the current, this concentration gradient is then allowed to relax, or equilibrate. As the cell relaxes, the cell potential gradually approaches zero. We then create a semi-log plot of cell potential vs. time and use the slope of the relaxation portion of the curve to find a line of best fit with the model. The line of best fit corresponds to a tortuosity value that is taken to be the apparent tortuosity. The model generates the relaxation curve by solving a mass transport differential equation in a 1D restricted-diffusion geometry using the finite element package COMSOL. The model uses intrinsic transport properties of the electrolyte to solve the mass transport equations. These intrinsic properties are obtained from the literature.[24]

Blocking-Electrolyte Method

The second method used to determine the tortuosity of battery electrodes is the blocking-electrolyte method developed by Landesfeind et al.[12] This method uses impedance measurements of electrodes in a symmetric cell with a non-intercalating electrolyte (Figure 3). A transmission-line model (TLM) is used to fit the resulting impedance curve on a Nyquist plot, allowing for determination of effective ionic resistance (R_{ion}) of the electrodes, which is then used to determine the MacMullin number and tortuosity of the electrodes according to Equation 2. Figure 4a shows an example of such experimental impedance data on a Nyquist plot that is a convenient shape for the blocking-electrolyte method.

Blocking conditions are obtained using an electrolyte salt that cannot substantially generate an electrochemical reaction with the electrodes at the operating potential. In this work, we refer to this non-intercalating electrolyte as a blocking electrolyte. This method is

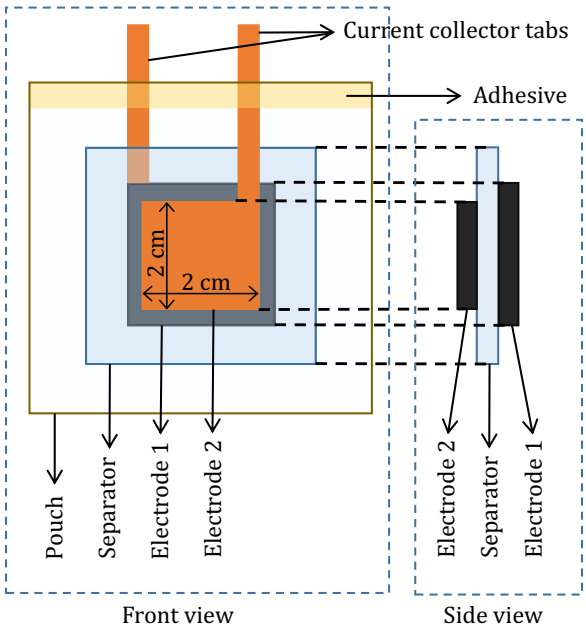

Figure 3. Schematic of blocking-electrolyte cell.

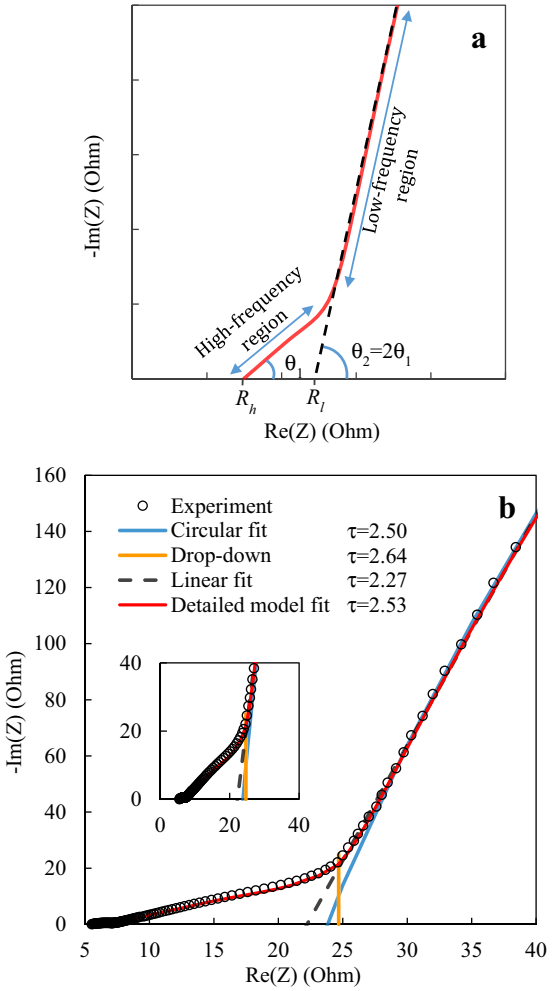

Figure 4. (a) Example of Nyquist impedance plot with reference to key characteristics and (b) the difference in simple tortuosity approximation methods, showing the effect on calculated tortuosity values.

effective because it creates an ideally polarized surface, meaning that there is no faradaic charge transfer across the solid/liquid interface, thus simplifying interpretation of the impedance spectrum.

Landesfeind et al. simplified the blocking electrolyte TLM by neglecting electronic resistance because of its typical small magnitude in comparison to ionic resistance (a fact confirmed by our own experiments).[27,28] Knowing R_{ion} based on this model, the effective conductivity can be determined based on the cross-sectional area of the cell (A), the thickness of the sample (l), and the intrinsic conductivity of the electrolyte (k_{int}):

$$N_{\text{M}} = \frac{\tau}{\epsilon} = \frac{R_{\text{ion}}\, A\, k_{\text{int}}}{l} \qquad [4]$$

Generalized transmission line model.—In this work, a more-detailed TLM model was developed to account for a wider range of physical possibilities. Figure 5 shows a diagram of the transmission-line model for the system. While the diagram indicates discrete resistances, the model is solved as a differential system. Equation 5 gives the resulting electrode impedance from the generalized transmission-line model, dependent on a variety of physical interactions:

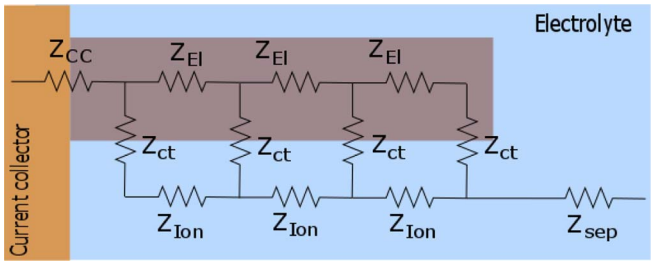

Figure 5. Diagram of the transmission-line model (Equation 5).

Table I. Definitions of the terms found in Equations 5 and 12.

Variable	Definition
Z_{EL}	Electrode Impedance
R_{ion}	Ionic Resistance
k_{eff}	Effective Ionic Conductivity
σ_{eff}	Effective Electronic Conductivity
z_{cc}	Contact Impedance of the Solid with the Current Collector
z_c	Contact Impedance of the Electrolyte with the Current Collector
z_s	Charge Transfer Impedance
L	Electrode Thickness
β	$\frac{k_{\text{eff}}}{\sigma_{\text{eff}}}$
Z_0	$\frac{z_c\, k_{\text{eff}}}{L}$
Z_{cc}	$\frac{z_{cc}\, k_{\text{eff}}}{L}$
λL	$L\sqrt{\frac{\sigma_{\text{eff}}+k_{\text{eff}}}{\sigma\, k_{\text{eff}}\, z_s}} = \sqrt{(1+\beta)\frac{R_{\text{ion}}}{Z_s}}$
Z_s	$\frac{z_s}{L \cdot area}$
c	$\cosh(\lambda L)$
s	$\sinh(\lambda L)$

The origin of this impedance solution is as follows. The governing equation for the conservation of electronic charge in the porous electrode is

$$0 = \sigma_{\text{eff}} \frac{d\varphi_1^2}{dx^2} + \frac{\varphi_2 - \varphi_1}{z_s} \qquad [6]$$

where φ_1 is the potential in the solid phase, φ_2 is the potential in the electrolyte phase, and z_s is the linearized impedance for charge transfer between these two phases. The governing equation for the conservation of ionic charge is likewise

$$0 = k_{\text{eff}} \frac{d\varphi_2^2}{dx^2} + \frac{\varphi_1 - \varphi_2}{z_s} \qquad [7]$$

The constitutive equations for electronic (i_1) and ionic (i_2) superficial current densities are:

$$i_1 = -\sigma_{\text{eff}} \frac{d\varphi_1}{dx} \qquad [8]$$

$$i_2 = -k_{\text{eff}} \frac{d\varphi_2}{dx} \qquad [9]$$

where σ_{eff} and k_{eff} are the effective conductivities in the solid and electrolyte phases, respectively. The boundary conditions at the current collector assume a reference potential of zero, such that:

$$i_1 = -\sigma_{\text{eff}} \frac{d\varphi_1}{dx} = \frac{0 - \varphi_1}{z_c} \qquad [10]$$

$$i_2 = -k_{\text{eff}} \frac{d\varphi_2}{dx} = \frac{0 - \varphi_2 - U}{z_{cc}} \qquad [11]$$

$$Z_{\text{EL}} = R_{\text{ion}} \frac{\left[\beta\,(Z_0 - Z_{cc}) + (1+\beta)\,Z_0 Z_{cc} + (1-\beta)\,(\lambda L)^{-2}\right]\,\lambda L \tanh(\lambda L) + (1 + 2\beta\,\text{sech}\,(\lambda L) + \beta^2) Z_0 + \beta\,(1-\beta)}{(1+\beta)\,(Z_0 - Z_{cc})\,\lambda L \tanh(\lambda L) + 1 - \beta^2} \qquad [5]$$

Table I defines the variables used in Equation 5.

where z_c is the contact impedance of the current collector in the solid phase, z_{cc} is the contact impedance of the current collector in the electrolyte phase, and U is the open circuit potential for the reaction of the electrolyte with the current collector relative to the potential of the faradaic reaction between electrolyte and active material. U is assumed to be zero hereafter, to simplify the solution. This is justified since i_2 at the current collector is close to zero due to the low surface area of the current collector. Additional boundary conditions at the separator ($x = L$) assume that the separator is electronically insulating ($i_1 = 0$), and that the electrolyte potential is fixed, $\varphi_1 = \varphi_2$. Finally, it is assumed that impedances are linear due to small potential perturbations and the assumption that concentration across the system is uniform in the absence of substantial faradaic reaction.

Any of the model parameters given above could be expressed as complex numbers. In general we take each of the z_s, z_c, and z_{cc} impedances as equivalent to a resistor parallel to a constant-phase element, and σ_{eff} and k_{eff} both as real-valued.

Solving these governing equations and boundary conditions one can obtain functions $\varphi_1(x)$ and $\varphi_2(x)$. When these are substituted back into Equations 8 and 9 and Ohm's law, one can solve for the overall impedance of the electrode:

$$Z_{EL} = \frac{R_{ion}}{L}\frac{c\,k_{eff}\,\lambda\,\left[L\,(k_{eff}-\sigma_{eff})-\left(k_{eff}^2+\sigma_{eff}^2\right)z_c\right]-s\,\sigma_{eff}\left[\left[L\,(z_c-z_{cc})+(\sigma_{eff}+k_{eff})\,z_c z_{cc}\right]k_{eff}^2\,\lambda^2+(\sigma_{eff}-k_{eff})\right]-2k_{eff}^2\,\sigma_{eff}\,\lambda\,z_c}{\lambda\,(\sigma_{eff}+k_{eff})\left[s\,\lambda\,\sigma_{eff}\,k_{eff}\,(z_{cc}-z_c)+c\,(k_{eff}-\sigma_{eff})\right]} \quad [12]$$

which reduces to Equation 5 by substituting the dimensionless ratios shown in Table I.

Once the assumption is made that there is no faradaic reaction at the current collector, (as discussed above, i_2 is small due to the low surface area) the boundary conditions presented here more closely match the boundary conditions used by Troltzch and Kanoun,[25] and the model results can be considered similar. Other works have developed impedance models for systems with diffusion by using the Warburg impedance.[29,30] Interestingly, the results using Warburg impedance produce similar impedance curves to those produced using the blocking-electrolyte method. Though the physics of the two cases are different, the resulting governing differential equations are similar and so too are the impedance spectra.

Here we discuss the assumptions which reduce Equation 5 to a form more commonly used for the blocking-electrolyte system. If we assume that electronic conductivity is much greater than ionic conductivity in our system ($\beta \ll 1$), then:

$$\lambda = \sqrt{\frac{1}{k_{eff}\,z_s}} \quad [13]$$

And, if we also assume that there is no effective faradaic reaction and no double-layer effect directly between electrolyte and the current collector ($Z_0 \gg 1$) then:

$$Z_{EL} = R_{ion}\left(Z_{cc} + \frac{1}{\lambda L \tanh(\lambda L)}\right) \quad [14]$$

This would be expected to be a reasonable assumption in most cases given that the surface area of contact between a largely planar current collector and the electrolyte is small relative to the amount of contact area elsewhere in the porous electrode.

Since we observed in our experiments that in some cases there *is* a significant electronic contact resistance between the electrode film and current collector it is useful to include Z_{cc} in modeling electrode impedance. This allows us to more accurately determine tortuosity for plots such as the one shown in Figure 6. However, if one additionally assumes that the electronic contact resistance between the sample and the current collector is negligible, then this reduces the model to a form equivalent to that used by Landesfeind et al. and by Ogihara et al.:[12–14]

$$Z_{EL} = \frac{R_{ion}}{\lambda L \tanh(\lambda L)} \quad [15]$$

Blocking conditions.—It is useful to examine the conditions under which there is no effective faradaic reaction on the surface of the active material in the porous electrode, i.e. when there is a "blocking condition." The current density of the faradaic reaction is dependent upon concentrations in the relevant phases.[30] The Butler-Volmer-type equation shown below is for the general lithium-ion surface reaction $Li^+ + e^- + \Gamma \leftrightarrow Li\Gamma$ where Γ is the unfilled lattice site and $Li\Gamma$ is the filled lattice site in the active material.

$$i = i_0^{ref}\left(\frac{C}{C_{ref}}\right)^{\alpha}\left(\frac{C_s}{C_{ref,s}}\right)^{\alpha}\left(\frac{C_{max}-C_s}{C_{ref,s}}\right)^{\alpha} \times\left[\exp\left(\frac{\alpha_a F\eta_s}{RT}\right)-\exp\left(-\frac{\alpha_c F\eta_s}{RT}\right)\right] \quad [16]$$

where i is the surface current density and other variables are defined in Table II. The concentration-containing terms are part of the exchange current density. Ogihara et al. obtained blocking conditions by testing cells at a state-of-charge (SOC) = 0% or 100%, where 0% SOC corresponds to $(C_s/C_{ref,s}) = 0$ and 100% SOC corresponds to $[(C_{max} - C_s)/C_{ref,s}] = 0$.

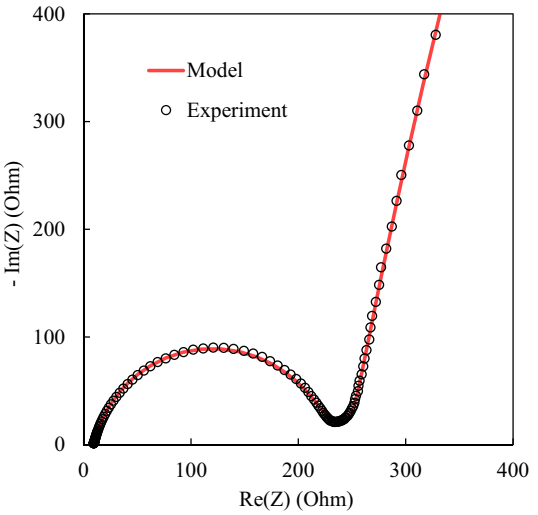

Figure 6. Example of Nyquist impedance plot of a pristine intact uncalendered cathode with relatively large contact resistance that obscures the high-frequency region, along with model fit using Equation 15.

Table II. Definitions of the variables in Equation 16 (a Butler-Volmer-type equation for current density in a lithium-ion reaction with a generic active material).

Variable	Definition
i	Current Density on surface of active material
i_0^{ref}	Reference Exchange Current Density
C	Concentration of Lithium in the Electrolyte
C_{ref}	Reference Concentration in the Electrolyte
C_s	Concentration of Lithium in the Solid active material
$C_{ref,s}$	Reference Concentration of Lithium in the Solid
C_{max}	Maximum concentration of lithium in solid when all active sites are filled
α_a	Anodic Charge Transfer Coefficient
α_c	Cathodic Charge Transfer Coefficient
F	Faraday's Constant
η_s	Anodic overpotential
R	Universal Gas Constant
T	Temperature

Table III. Thickness and porosity values for commercial cathodes and anodes measured using both the polarization-interrupt and blocking-electrolyte methods.

Electrode	Thickness (microns)	Porosity (%)
Cathode 1 (Hydro-Quebec LCO)	45	17
Cathode 2 (TMO)	87	36
Cathode 3 (TMO)	60	36
Anode (Graphite)	115	36

Landesfeind et al. found that by using a blocking electrolyte (the concentration of lithium in the electrolyte is negligible) the faradaic current density is also negligible because $(C/C_{\text{ref}}) = 0$. Thus, Landesfeind et al. produce a more robust blocking condition that does not depend on the state of charge of the active material. Nevertheless, we observed that, even while using blocking electrolyte, a slight faradaic reaction can often be observed. This less-than-ideal blocking condition is manifested by a slight curvature in the low-frequency portion of the Nyquist curve. This could be due to Li ions coming from active materials or, in the case of non-pristine electrodes, from residual Li-containing salt, or from unintended intercalation or reaction of components of the blocking electrolyte. In any case, the generalized transmission line model developed above may be used to account for non-ideal systems such as these.

Experimental

Electrodes.—We measured 3 commercially supplied transition metal oxide (TMO) cathodes. Hydro-Quebec also provided a lithium cobalt oxide (LCO) cathode with known composition of 93% active material, 4% carbon, and 3% binder by weight. We also measured a single commercial graphite anode. Table III gives the thickness and porosity for each of the electrodes measured. The porosities are either reported by the supplier or estimated using typical porosities for commercial electrodes (note that reported MacMullin numbers do not depend on these values).

Electrode delamination.—Some cells, primarily for the polarization-interrupt method, required prior delamination of the electrode films. This was achieved by using 45wt% aqueous potassium hydroxide solution for cathodes and a standard acid solution (either 1M nitric acid or 1M hydrochloric acid) for anodes. Different electrodes may require different concentrations of acid or base. Acid or base concentrations were chosen in order to delaminate the electrodes in a reasonable amount of time without damaging the electrode structure. Figure 7 shows steps for delaminating an anode film. A 2.5 × 2.5 cm electrode is placed in a petri dish and 0.5 mL of acid solution is placed on the electrode, forming a large drop. A glass plate is placed on top of the electrode and drop (see Figure 7b) in order to flatten the electrode during the delamination process and avoid wrinkles or cracks. The electrode is then allowed to soak for few minutes until the electrode coating delaminates from the current collector (Figure 7c). The electrodes were then rinsed by soaking carefully with distilled water repeatedly. The electrodes were then allowed to dry. A similar process was followed for cathode films using potassium hydroxide solution; however, it was necessary to wait for the aluminum layer to completely dissolve in solution in order to separate the electrode films. In order to avoid aluminum residue on the films after drying it is necessary to re-apply the basic solution after the first rinse. The cathode films are then rinsed repeatedly as with anode films and allowed to dry. In our experience, the above aqueous treatments do not have a significant effect on electrodes based on PVDF binder.[10] Obviously this delamination procedure is not recommended for electrodes based on water-soluble binder.

Symmetric-pouch-cell assembly.—The delaminated electrodes were transferred into an argon atmosphere glove box (moisture content 0.9ppm and oxygen content <0.025ppm, VAC, Hawthorne, CA). The electrodes were then placed as a freestanding film in between two separator layers (Celgard 3501, Celgard LLC, Charlotte, NC). The film and separators were then sandwiched between two pieces of (approximately 4 cm^2) lithium metal foil (Alfa Aesar) that had been pressed onto copper current collectors. One Li foil is sized slightly larger than the other in order to minimize alignment difficulty–the smaller of the two foils constitutes the controlling electrode surface area. The entire cell was placed into a metalized polymer film (Figure 2a). An electrolyte solution of 1 M lithium hexafluorophosphate in a 50/50 (v/v) mixture of ethylene carbonate and diethyl carbonate was injected into the pouch. The pouch was then sealed using an electric

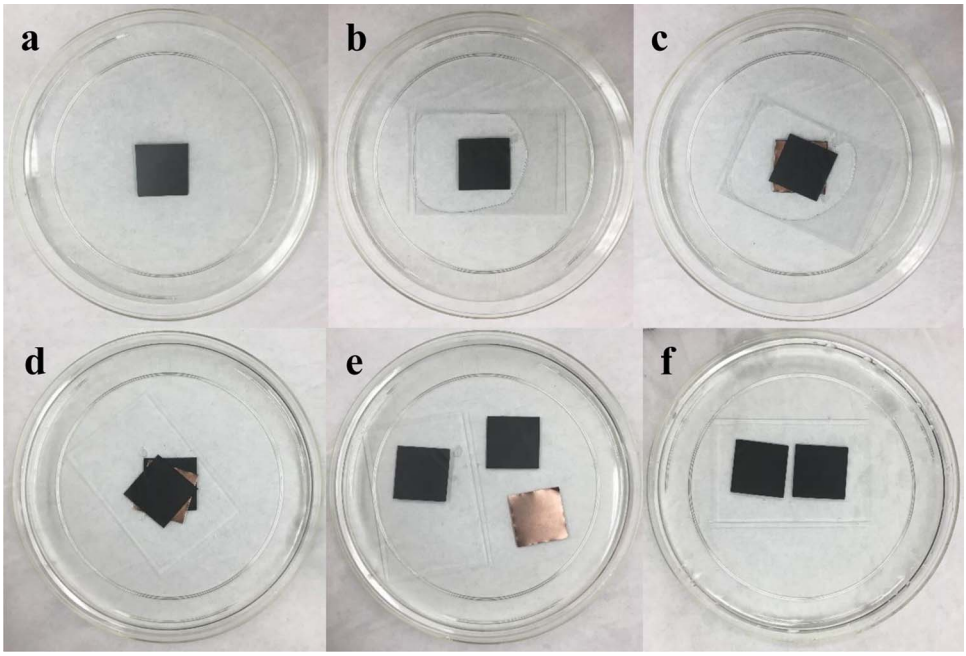

Figure 7. Delamination process of a (2.5 × 2.5) cm^2 Anode using nitric acid.

heat sealer (Impulse Sealer Tish 200, Electronic Heating Equipment Co.).

In order to make blocking-electrolyte cells, electrodes and separator were placed into a pouch cell according to the configuration shown in Figure 3. A 4 cm^2 electrode and a second larger electrode were cut. As discussed above, the difference in size is for convenience in aligning the two electrodes. The total effective area of the cell is 4 cm^2 so that the cell is essentially symmetric. A separator was placed between these electrodes and the stack was placed into the pouch (Figure 3). Uncoated current collector protruded outside the sealed pouch and was used as an electrical connection. An electrolyte of 20mM tetrabutylammonium hexafluorophosphate ($TBAPF_6$) in a 1:1 (w:w) mixture of ethylene carbonate (EC) and dimethyl carbonate (DMC) was added to the pouch cell and the cell was sealed using a heat sealer. We also tested blocking-electrolyte cells using $TBAPF_6$ in a mixture of propylene carbonate and EC as well as $TBAClO_4$ (tetrabutylammonium perchlorate) in a DMC/EC mixture. The results of these tests indicated that only slight variations in tortuosity measurement resulted from changing electrolyte mixtures. We chose $TBAPF_6$ in DMC/EC because of its similarity to the electrolyte used in commercial Li-ion cells. All of the salts and solvents used in these tests were obtained from Sigma Aldrich.

Cell testing.—Polarization-interrupt cells were tested using a Maccor 4300. The cells were first cycled several times to form an SEI layer on the Li metal. The formation cycle includes passing a constant current (0.5 mA/cm^2) for 10 minutes followed by 3 minutes relaxation. In every other cycle, the current direction is changed in order to maintain symmetry in the cell. After the formation cycles were completed, the cell was polarized by passing a fixed current (either 0.75, 1, or 1.25 mA/cm^2) through the cell for 2 minutes. The current was then turned off or interrupted. After interruption of the current, the system was then allowed to equilibrate for several minutes. As the cell relaxes, the cell potential gradually approaches zero. The test was then repeated with current in the opposite direction. Relaxation curves for multiple experiments were averaged and then fit to a diffusion model as described in prior work.[19]

We tested our blocking-electrolyte cells by following the method developed by Landesfeind et al. for determining tortuosity. Using a Bio-Logic SP-200 potentiostat, EIS measurements were taken near the open circuit voltage of each cell. An appropriate frequency range with a 10 mV perturbation was used. Generally a frequency range of 0.5 Hz to 500 kHz provides an appropriate Nyquist spectrum, however depending on the sample it might be required to choose a wider frequency range. The widest range we used was 0.1 Hz to 3 MHz.

Both polarization-interrupt and blocking-electrolyte tests were run after allowing the cell to sit for approximately 24 hours to ensure that the sample was completely wetted. Cells were tested under an external pressure of approximately 45 kPa, produced by placing a rubber layer and a metal weight on top of the pouch cell.

Both methods were repeated by making a new pouch cell for each test, in order to obtain 95% confidence intervals. For Figure 8 tests were repeated for 8 cells for blocking-electrolyte and 5–7 cells for polarization-interrupt methods. The maximum uncertainty in tortuosity values obtained for blocking-electrolyte and polarization-interrupt methods were 5% and 12%, respectively. For other results noted below, fewer repetitions were performed. For some cases, due to lack of sufficient materials, repetitions were not performed; for these cases uncertainty can be estimated based the above general uncertainties in the methods. Furthermore, the model was not considered as a significant source of uncertainty; based on our experience, we expect more uncertainty from one sample to the next rather than any particular model fit.

Results and Discussion

Polarization-interrupt and blocking-electrolyte values for tortuosity are shown side-by-side in Figure 8. The results show reasonable

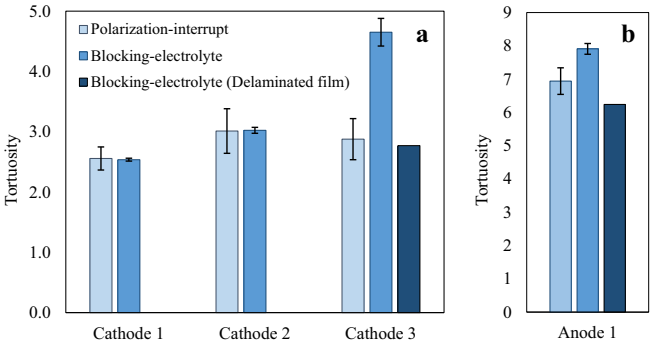

Figure 8. Comparison of tortuosity values for polarization-interrupt and blocking-electrolyte methods for (a) commercial quality transition metal oxide cathodes and (b) a commercial quality graphite anode. 95% confidence intervals are shown, except in the case of blocking electrolyte (delaminated film).

agreement between the two methods. This result validates both methods and confirms that tortuosity values are larger than predicted by a conventional Bruggeman-type relationship, as previously reported by our group.[10,24] Of note, both Cathode 3 and the Anode show apparent disagreement between the two methods. We observed that the delamination process resulted in increased thickness for these two samples (12% for cathode 3 and 5% for the anode). This increase in thickness results in increased porosity of the electrodes and this may contribute to the apparent disagreement in tortuosity since nominal (dry) thickness and porosity values were used to calculate tortuosity, according to customary practice. In order to better compare the two methods using delaminated films for both methods, delaminated films were tested using the blocking-electrolyte as explained in the section below. Comparing the two methods for the delaminated films again establishes reasonable agreement.

Slight differences between tortuosity values from diffusivity and tortuosity values from conductivity could be attributed to nanoscale effects. Transport theory shows that, assuming no interactions between the electrolyte and the walls of the pores (i.e. bulk behavior), tortuosity values obtained from conductivity and diffusion will be the same. On the other hand, electrokinetic theory suggests that there could be slight differences in these values if enough electrolyte is present in nanoscale pores, such that a large fraction of the ions in these pores is found in the electrochemical double layer.[6] To make a quick estimate of such a possibility, one could compare a typical pore diameter with the Debye length for the electrolyte. If the smallest pore diameters in battery electrodes are on the order of typical carbon black diameter (around 50 nm), and the electrolyte Debye length is around 0.3–2 nm (for the range of concentrations used in this work), then approximately 1–8% of the ions in those pores would be within one Debye length of any pore wall. Again this suggests only a small effect would be possible. Nevertheless, in this work tortuosity values by diffusion and conduction experiments have reasonable agreement. Any differences are within experimental uncertainty, making it difficult to attribute such differences to possible nanoscale or double-layer effects.

Blocking-electrolyte method.—Blocking-electrolyte data is fit by a least squares fit, namely by minimizing the objective function shown below (Eq. 17) which results from the generalized transmission-line model (Eq. 5) discussed above

$$F = \sum_{n=1} \frac{(|Z_t - Z|)^2}{|Z_t|^p} \qquad [17]$$

where Z_t is the experimental impedance at a particular frequency and Z is the corresponding impedance given by the model for the symmetric pouch cell:

$$Z = 2Z_{EL} + R_{sep} \qquad [18]$$

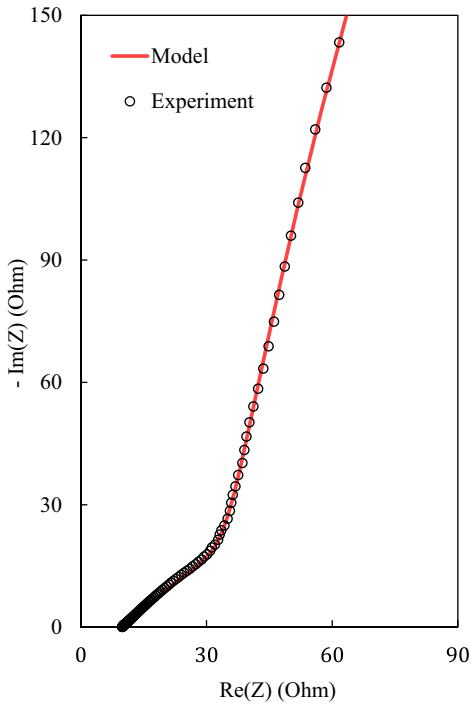

Figure 9. Example of Nyquist impedance plot of blocking electrolyte experiment with model fit for a cathode sample.

The objective function minimizes the error between the electrode impedance of the model (Z_{EL}) and the experimental impedance data (Z_t). It was found empirically that normalizing or weighting the errors (by means of the denominator in Eq. 17, including the exponent p) improved the robustness of the fit. By robustness we mean that model and experiment match well in the intermediate-frequency "elbow" region of the Nyquist plot, in order to determine the best value of R_{ion}. Different values of exponent p were tested, and generally $p = 0.01$ worked well. Other weighting schemes are possible and can affect the regressed parameters.[31] Figure 9 shows an example fit to experiment using our recommended objective function.

Figure 4a is a schematic that emphasizes some key points, discussed below, in fitting the Nyquist plots generated from the blocking-electrolyte experiment. Firstly, the angle of the Nyquist curve in relation to the real impedance axis in the high frequency region is twice the angle in the low frequency region, i.e. on either side of the "elbow." This relationship is also reflected in the dependence that both the high frequency and low frequency portions of the Nyquist curve have on parameter γ_s. This double-angle relationship can aid in trying to get an adequate model fit when experimental results are less ideal. Secondly, as the blocking conditions become less ideal the low-frequency portion of the Nyquist plot exhibits greater curvature due to the influence of faradaic reaction at these low frequencies. While this curvature is accounted for in the general model, it is problematic when attempting to find a quick graphical approximation of tortuosity as explained below.

Approximating ionic resistance.—Although fitting the full impedance spectrum to the mathematical model is a more reliable way to get an accurate ionic resistance (R_{ion}), there are some quick approximation methods that can give us a reasonable estimate of R_{ion}. As shown in Figure 4a, the difference between the high-frequency intercept R_h and the low-frequency intercept R_t is approximately $R_{ion}/3$. Ogihara et al. proposed a "drop-down method" meaning that the low-frequency intercept is simply the real impedance at the elbow of the Nyquist plot. This method can be problematic because of the difficulty in identifying which point of a continuous impedance spectrum should be projected down to the real axis. Landesfeind et al. used a transmission-line-model to determine R_{ion} but suggested that a quick approximation can be found by a linear extrapolation of the low-frequency portion of the Nyquist plot. As discussed above, however, the low-frequency region is not always a straight line but frequently has some curvature due to faradaic reaction. One improvement to the linear approximation suggested by Landesfeind et al. may be to account for the curvature of the low-frequency region in determining the low-frequency intercept value. This is done by using a circular rather than linear fit in the low-frequency region. Figure 4b shows the approximated tortuosity values using these three methods as compared to using our detailed model.

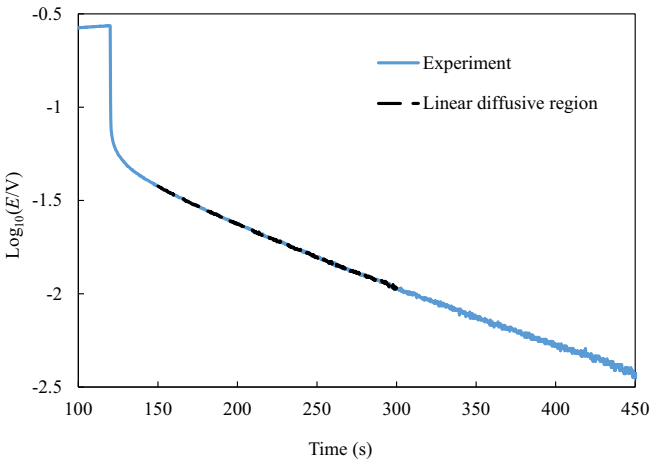

Figure 10. Example of cell potential during polarization-Interrupt experiment. The black dashed line shows part of the data taken to be the linear diffusive region.

Polarization-interrupt method.—Figure 10 shows a typical relaxation curve for the polarization-interrupt method. The region marked in black indicates the portion of the curve which is taken to be the linear diffusive region. This region is chosen to minimize the influence of random noise as well as possible small DC bias potential, both of which impact the diffusive relaxation signal at longer times. On the other hand, at too short of times fully diffusive behavior has not begun. Therefore, based on multiple experiments the time range indicated in the figure was chosen for the fit. The slope of this linear diffusive region is measured and the model (developed by Thorat et al.)[24] is used to find the tortuosity corresponding to the slope that best matches this measured slope.

Method comparison.—While both polarization-interrupt and blocking-electrolyte methods return comparable values of tortuosity, it may be more convenient to apply one method rather than the other for particular electrodes. For example, the blocking-electrolyte method is generally faster and more convenient; however, for some cases the generated Nyquist plot does not lend itself to easy quantitative analysis. Figure 11 shows, as an example, the Nyquist plot of an anode harvested from a cycled cell and that cannot be analyzed under the blocking-electrolyte method due to an abnormal shape. The harvested electrode has been rinsed with dimethyl carbonate multiple times to make sure there is no salt residue remaining to interfere with the blocking condition. A definitive conclusion on possible causes for this abnormal shape is beyond the scope of this work.

Figure 6 shows the Nyquist plot for a non-commercial cathode for which the high-frequency region is obscured by a semicircle attributed to contact resistance.[12,32] The detailed model presented in this work can account for this contact resistance, allowing effective ionic resistance to be determined, albeit with increased uncertainty. An alternative for cases with large contact resistance is to reduce electrolyte conductivity, which may de-convolute electronic and ionic effects and allow ionic resistance to be clearly observed. Figure 12 illustrates this,

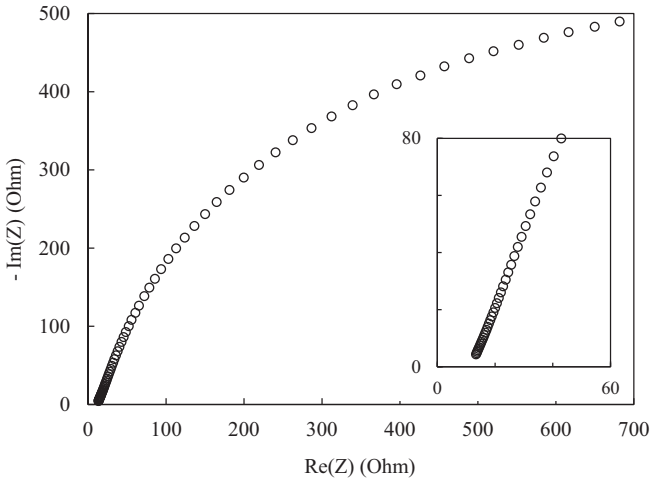

Figure 11. Nyquist impedance plot of blocking electrolyte method for cycled anode. The inset shows behavior at high frequencies.

showing how the overlap between electronic and ionic impedances at high frequency is reduced. While this solution may be useful in some cases, one should consider that making electrolyte conductivity too low may introduce other difficulties. For instance, at very low concentration, electrolytes are more sensitive to impurities, and conductivity variation due to possible solvent evaporation during pouch assembly is more pronounced. A third alternative for dealing with cases of large contact resistance, namely delamination and replacement of the current collector, is described below.

Some concerns with using the polarization-interrupt method may arise from issues with delamination of thin films that can easily be damaged during this step (Figure 13). While thin films can be delaminated, it can require more time, lower concentration acid or base solution, and great care. In addition, films with low tortuosity compared to the tortuosity of the separator layers can increase error since it can be difficult to distinguish small variations in separator tortuosity from the tortuosity of the film. A related problem is that thin films (i.e. with small diffusion time constants) may not exhibit a sufficiently linear diffusive region to enable accurate matching to the transport model. As shown in Figure 2b, this particular problem can be overcome by using multiple stacked layers of the delaminated film

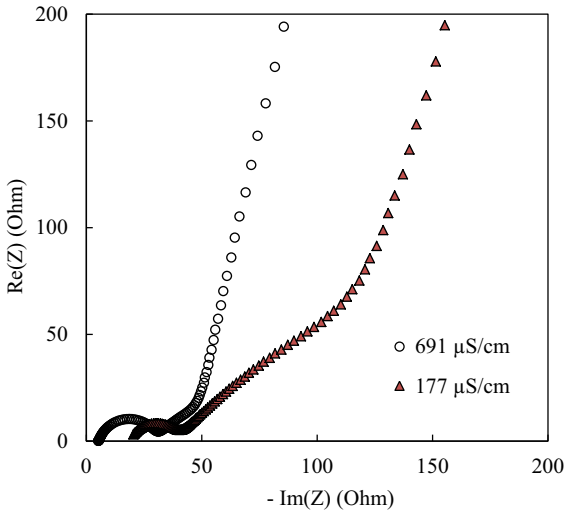

Figure 12. Example of Nyquist impedance plot of a cathode, using electrolytes with different conductivities, showing the effect of lower conductivity electrolyte in de-convoluting ionic from electronic contact resistances.

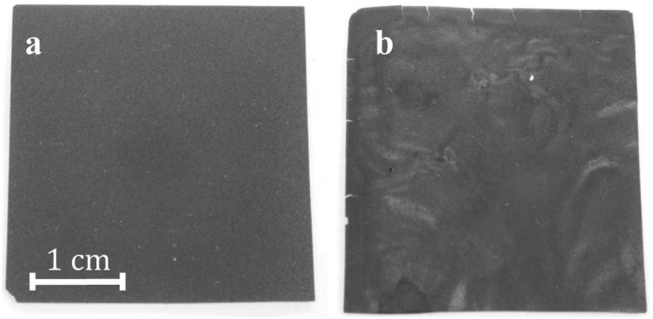

Figure 13. Photographs of delaminated (a) intact film and (b) film damaged by delamination.

to increase the diffusive resistance of the sample relative to that of the separators.

Both tortuosity measurement methods can also be sensitive to the amount of wetting, electrolyte leakage from the cell, and evaporation of the electrolyte during assembly. Efforts were made here to minimize these effects. Furthermore, variation in the blocking-electrolyte method due to evaporation can be normalized by using the high frequency intercept of the Nyquist plot as an internal reference to determine the intrinsic conductivity of the electrolyte. This requires knowing the MacMullin number of the separator so that the intrinsic conductivity of the electrolyte can be determined in situ.

The tortuosity of the separator (Celgard 3501) was measured using the AC impedance method explained by Thorat et al.[24] Here the method was implemented in pouch cells with 4 cm^2 stainless steel electrodes, $TBAPF_6$ electrolyte, and multiple (2, 4, 6, or 8) layers of separator. The tortuosity for this separator was determined to be 3.24 from the linear fit to experiments with differing numbers of separators. The single-layer thickness and porosity are reported to be 25 µm and 55% respectively.

Blocking-electrolyte with delaminated film.—Large semi-circles in the high frequency region of the Nyquist plot (i.e. large contact resistance) were only observed for cathodes, which have an aluminum current collector, rather than for anodes, which have a copper current collector. We observed that when the same slurry is coated on both aluminum and copper foils, the electrode with the aluminum current collector may show significant contact resistance and yet there is no contact resistance for the equivalent film on copper. This observation further supports the idea that the semi-circle in the high frequency region of the Nyquist plot is due to contact resistance between the electrode film and current collector, as also concluded by Landesfeind et al.[12] and Gaberscek et al.[32] The loss of contact between current collector and electrode film for cathodes can be attributed to nonconductive oxidized aluminum at the interface of the electrode film and the current collector.

As mentioned above, to eliminate this problem and enable reliable ionic resistance measurement we tested the idea of delaminating a cathode from its aluminum current collector and replacing it with freestanding copper foil in the blocking electrolyte pouch cell. Figure 14 shows how contact resistant significantly decreases by replacing aluminum with copper in this manner. This is for an uncalendered cathode film. The resulting Nyquist plot can be used to reliably calculate tortuosity of the cathode. The tortuosity of Cathode 1 (Hydro-Quebec LCO) was tested for both the intact cathode (aluminum current collector) and for the delaminated cathode using copper as the current collector. Since the Nyquist plot using the intact cathode did not exhibit a large semi-circle in the high-frequency region, we conducted this test in order to validate that delamination does not have significant effect on the tortuosity of the sample. Figure 15 shows reasonably good agreement between these two methods. For Figures 14a, 14b, and 15b the number of tests to determine error bars were each 3. Figure 15a presents results previously given in Figure 8.

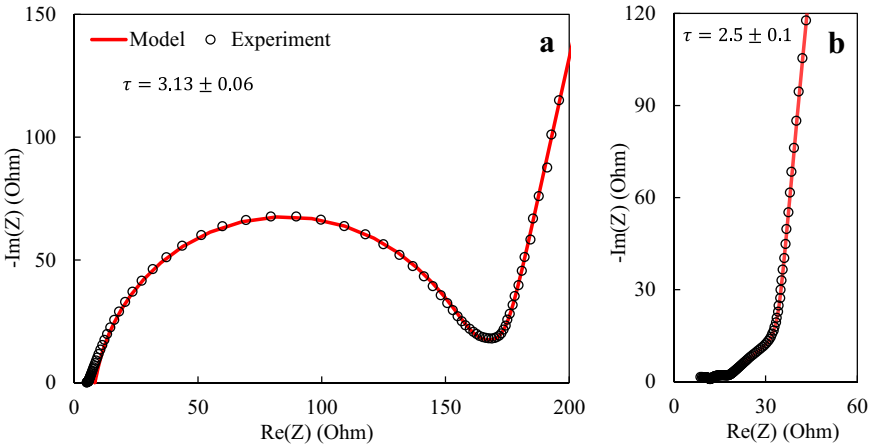

Figure 14. Nyquist plot of the blocking-electrolyte test for (a) intact cathode exhibiting large contact resistance and (b) delaminated cathode with copper as a current collector resulting in small contact resistance. Fitted tortuosity values and 95% confidence intervals are indicated on the plots.

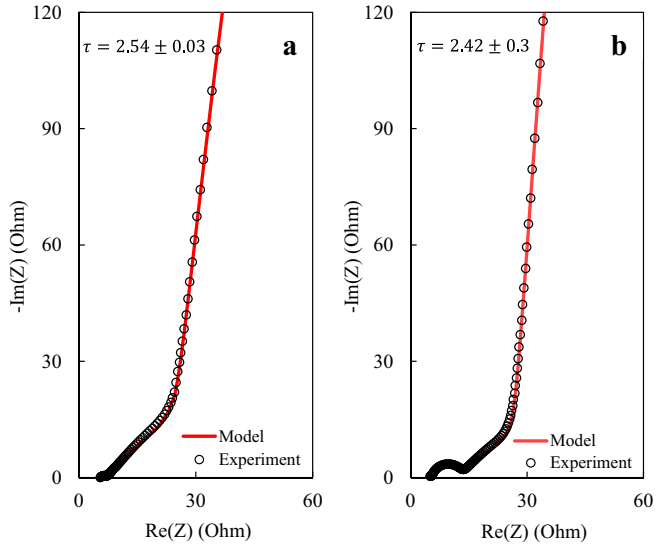

Figure 15. Nyquist plot of the blocking-electrolyte test for cathode 1: (a) intact and (b) delaminated with copper as a current collector. Fitted tortuosity values and 95% confidence intervals are also shown.

Conclusions

Battery models are useful tools in understanding how manufacturers and researchers can improve battery performance. Accurate tortuosity values are an essential input for any complete model of Li-ion battery performance. The polarization-interrupt method and blocking-electrolyte method are two effective ways for direct measurement of the tortuosity of Li-ion electrode films and are discussed and compared in this work.

The polarization-interrupt method, previously developed by our group, measures electrode-film tortuosity in terms of effective diffusivity. This is accomplished by building up a concentration gradient of ions in the film using a DC current and then interrupting the current and determining diffusivity using the slope of the relaxation curve. The blocking-electrolyte method, developed by Gasteiger and coworkers, is an alternative method for direct measurement of electrode-film tortuosity. This method uses AC impedance and a transmission-line-model to determine effective conductivity of a cell under blocking conditions.

The model used by Gasteiger and coworkers is a simplified transmission-line-model. In this work we propose a transmission-line-model that accounts for additional physical phenomena including impedance due to contact resistance between the current collector and the electrode film. This model can be adapted to account for a wider range of physical possibilities than models previously available in the literature.

In this work the tortuosity of several commercial electrodes were tested using both methods to compare and validate the results. Tortuosity values obtained through the blocking-electrolyte method are generally in agreement with those obtained through the polarization-interrupt method. This effectively validates both methods for direct measurement of tortuosity. Both methods are helpful since neither method is useful for every type of electrode film. In future work we will use these techniques to study the effect of variables such as cycling and mixing processes on the tortuosity of electrode films.

Acknowledgments

Funding for this research was provided through the BMR project of the US Department of Energy (DOE Project Number DE-AC02-05CH11231). We would also like to acknowledge Chisu Kim of Hydro- Québec and Bryant Polzin of the CAMP facility at Argonne National Laboratory for providing electrodes for testing.

ORCID

Fezzeh Pouraghajan https://orcid.org/0000-0002-9636-6714
Dean Wheeler https://orcid.org/0000-0001-5017-3194

References

1. S. Flandrois and B. Simon, *Carbon*, **37**(2), 165 (1999).
2. M. S. Whittingham, *Chemical reviews*, **104**(10), 4271 (2004).
3. B. Scrosati, *Electrochimica Acta*, **45**(15–16), 2461 (2000).
4. J. W. Fergus, *Journal of Power Sources*, **195**(4), 939 (2010).
5. H. Li, Z. Wang, L. Chen, and X. Huang, *Advanced materials*, **21**(45), 4593 (2009).
6. J. Newman and K. E. Thomas-Alyea, *Electrochemical systems*, John Wiley & Sons (2012).
7. V. D. Bruggeman, *Annalen der physik*, **416**(7), 636 (1935).
8. R. MacMullin and G. Muccini, *AIChE Journal*, **2**(3), 393 (1956).
9. E. Robert and C. W. Tobias, *Journal of the Electrochemical Society*, **106**(9), 827 (1959).
10. N. A. Zacharias, D. R. Nevers, C. Skelton, K. Knackstedt, D. E. Stephenson, and D. R. Wheeler, *Journal of The Electrochemical Society*, **160**(2), A306 (2013).
11. B. Tjaden, D. J. Brett, and P. R. Shearing, *International Materials Reviews*, **63**(2), 47 (2018).
12. J. Landesfeind, J. Hattendorff, A. Ehrl, W. A. Wall, and H. A. Gasteiger, *Journal of The Electrochemical Society*, **163**(7), A1373 (2016).
13. N. Ogihara, Y. Itou, T. Sasaki, and Y. Takeuchi, *The Journal of Physical Chemistry C*, **119**(9), 4612 (2015).
14. N. Ogihara, S. Kawauchi, C. Okuda, Y. Itou, Y. Takeuchi, and Y. Ukyo, *Journal of The Electrochemical Society*, **159**(7), A1034 (2012).
15. S. Malifarge, B. Delobel, and C. Delacourt, *Journal of The Electrochemical Society*, **164**(11), E3329 (2017).
16. T. DuBeshter, P. K. Sinha, A. Sakars, G. W. Fly, and J. Jorne, *Journal of The Electrochemical Society*, **161**(4), A599 (2014).
17. D. Kehrwald, P. R. Shearing, N. P. Brandon, P. K. Sinha, and S. J. Harris, *Journal of The Electrochemical Society*, **158**(12), A1393 (2011).

18. C. J. Bae, C. K. Erdonmez, J. W. Halloran, and Y. M. Chiang, *Advanced materials*, **25**(9), 1254 (2013).
19. T. Hutzenlaub, A. Asthana, J. Becker, D. Wheeler, R. Zengerle, and S. Thiele, *Electrochemistry Communications*, **27**, 77 (2013).
20. S. Cooper, D. Eastwood, J. Gelb, G. Damblanc, D. Brett, R. Bradley, P. Withers, P. Lee, A. Marquis, and N. Brandon, *Journal of Power Sources*, **247**, 1033 (2014).
21. G. Inoue and M. Kawase, *Journal of Power Sources*, **342**, 476 (2017).
22. M. Ebner and V. Wood, *Journal of The Electrochemical Society*, **162**(2), A3064 (2015).
23. L. Zielke, T. Hutzenlaub, D. R. Wheeler, I. Manke, T. Arlt, N. Paust, R. Zengerle, and S. Thiele, *Advanced Energy Materials*, **4**(8), 1301617 (2014).
24. I. V. Thorat, D. E. Stephenson, N. A. Zacharias, K. Zaghib, J. N. Harb, and D. R. Wheeler, *Journal of Power Sources*, **188**(2), 592 (2009).
25. U. Tröltzsch and O. Kanoun, *Electrochimica Acta*, **75**, 347 (2012).
26. H. Göhr, *Advances in Electrochemical Applications of Impedance Spectroscopy*, p. 2, ZAHNER-elecktrik GmbH & Co., Aug. (1997).
27. S. W. Peterson and D. R. Wheeler, *Journal of The Electrochemical Society*, **161**(14), A2175 (2014).
28. B. J. Lanterman, A. A. Riet, N. S. Gates, J. D. Flygare, A. D. Cutler, J. E. Vogel, D. R. Wheeler, and B. A. Mazzeo, *Journal of The Electrochemical Society*, **162**(10), A2145 (2015).
29. J. Bisquert, G. Garcia-Belmonte, P. Bueno, E. Longo, and L. Bulhoes, *Journal of Electroanalytical Chemistry*, **452**(2), 229 (1998).
30. J. Bisquert, *The Journal of Physical Chemistry B*, **106**(2), 325 (2002).
31. A. Lasia, *Electrochemical impedance spectroscopy and its applications*, Springer (2014).
32. M. Gaberscek, J. Moskon, B. Erjavec, R. Dominko, and J. Jamnik, *Electrochemical and Solid-State Letters*, **11**(10), A170 (2008).